Properties of cosmic rays at energies $E > 100$ TeV

Composition resolution in air shower experiments

$$X_{max}^{A} = X_{max}^{P} - X_0 \ln A$$

$$\frac{N_e}{N_\mu} \approx 35.1 \left(\frac{E_0}{A \cdot 1\,\mathrm{PeV}}\right)^{0,15} \Leftrightarrow \lg\left(\frac{N_e}{N_\mu}\right) = C - 0,065 \ln A$$

assume $\Delta \ln A = 1$

$\Rightarrow \Delta X_{max} = 37\ \mathrm{g/cm^2}$

$\Rightarrow \Delta \frac{N_e}{N_\mu} \approx 16\,\%$

} realistic values for modern experiments

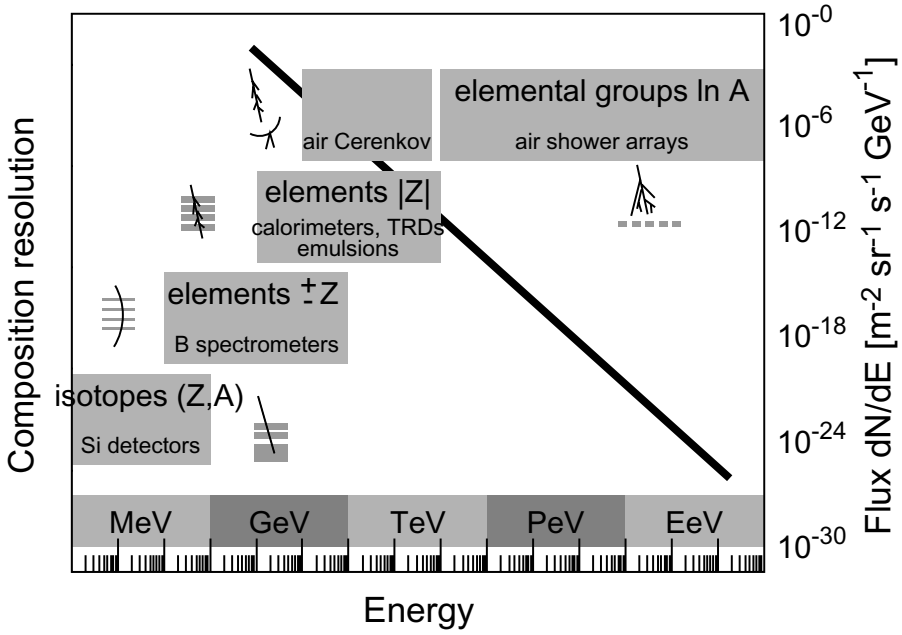

Fig. 1. Illustrative sketch of the composition resolution achieved by different cosmic-ray detection techniques as function of energy. Over the energy range shown the flux of cosmic rays decreases by about 30 orders of magnitude as indicated on the right-hand scale.

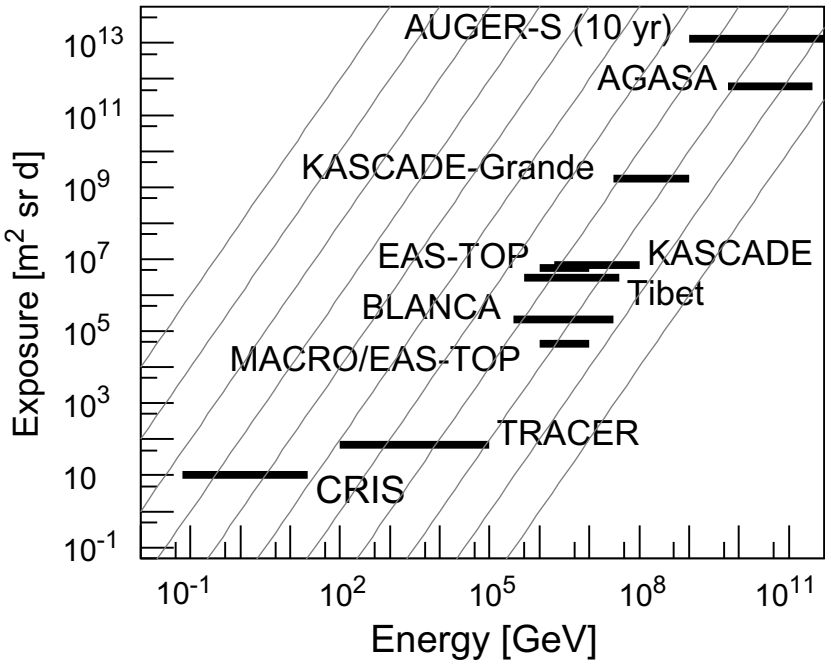

Fig. 2. Exposure of cosmic-ray experiments as function of energy for CRIS (Yanasak et al., 2001), TRACER antarctic and Sweden LDB flights (Hörandel, 2006a; Boyle, in press), MACRO/EAS-TOP (Aglietta et al., 2004b), BLANCA (Fowler et al., 2001), Tibet (Amenomori et al., 2003), EAS-TOP (Aglietta et al., 1999), KASCADE (Antoni et al., 2005), KASCADE-Grande (estimated 3 yr) (Navarra et al., 2004), AGASA, and AUGER south estimated 10 yr (Abraham et al., 2004). The grey lines are $\propto E^{-2}$.

e.g. KASCADE-experiment

$\Delta \ln A \approx 0{,}8$

$\Rightarrow$ 5 groups of elements

see below

Galactic cosmic rays and the knee in the energy spectrum

In air shower experiments detailed simulations are used to derive energy and mass of the primary particle.

$(N_e, N_\mu, N_h, s_e, s_\mu, s_h, N_\nu, \ldots) \xleftrightarrow{\text{simulations}} (\bar{E}, A)$

The simulations describe in detail the development of the particle cascades in the atmosphere.

complex calculations

- interactions of particles
- decay
- density profile of atmosphere
- B field of Earth

Results: all-particle energy spectrum

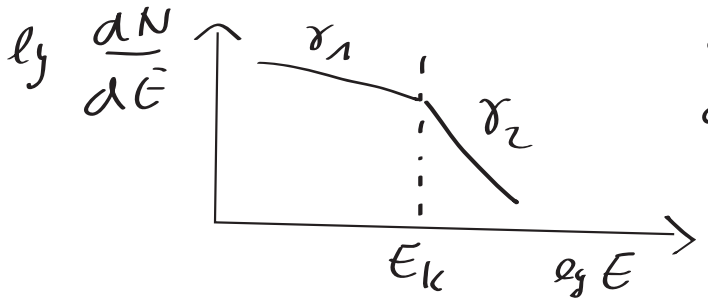

$$\frac{dN}{dE} \propto E^{\gamma}$$

$\gamma_1 \sim -2{,}7$

$\gamma_2 \sim -3{,}1$

$E_k \sim 4 \cdot 10^{15}\ eV$

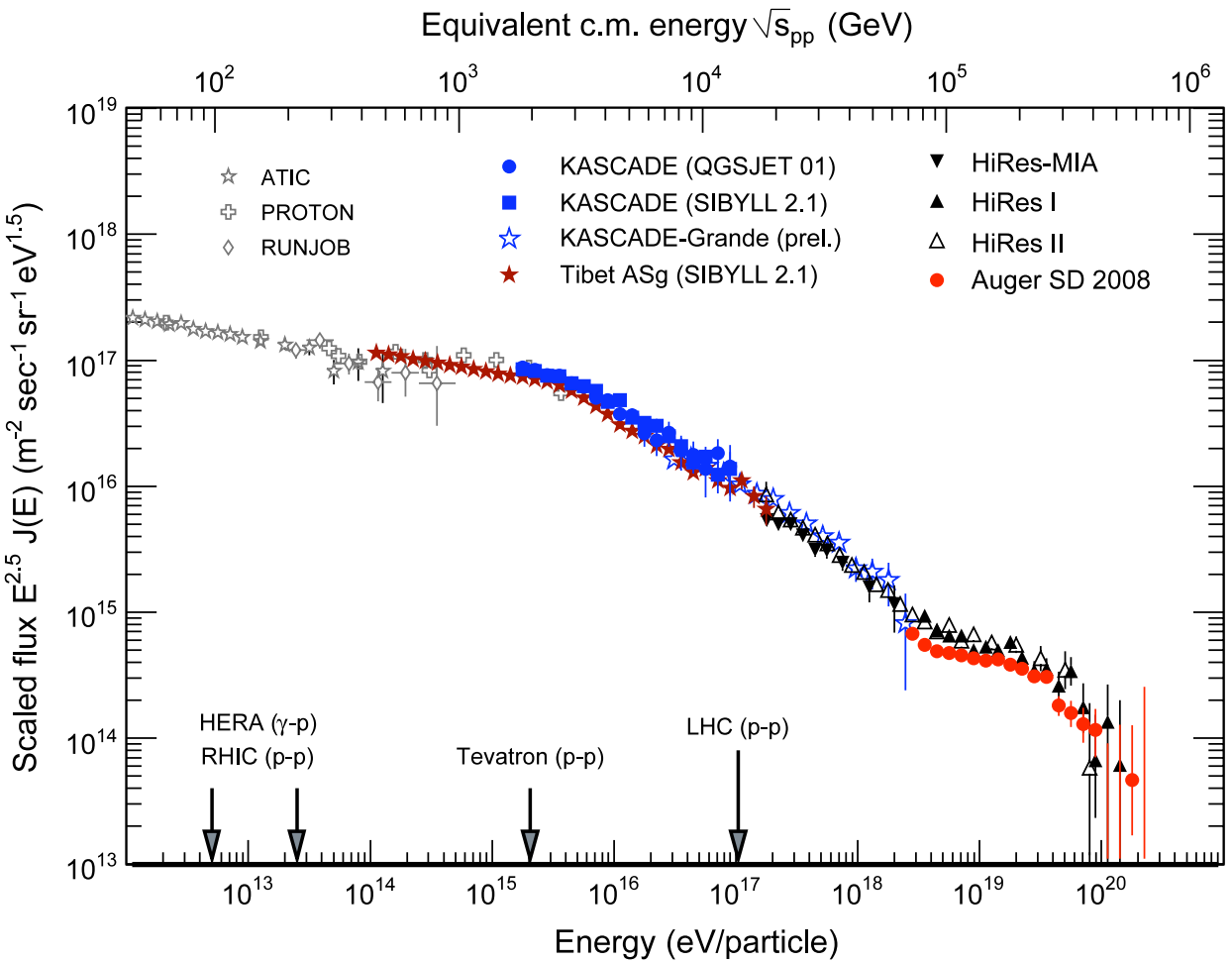

Fig. 7. All-particle cosmic-ray energy spectrum as obtained by direct measurements above the atmosphere by the ATIC [219,220], PROTON [221], and RUNJOB [222] as well as results from air shower experiments. Shown are Tibet ASγ results obtained with SIBYLL 2.1 [223], KASCADE data (interpreted with two hadronic interaction models) [224], preliminary KASCADE-Grande results [225], and Akeno data [226,33]. The measurements at high energy are represented by HiRes-MIA [227,228], HiRes I and II [229], and Auger [169].

Table 3
Air shower experiments and components measured to derive the primary energy spectrum

Experiment	e	μ	h	Č	F	g/cm^2	Energy shift (%)
AKENO (low energy) [73]	×	1 GeV				930	−4
BLANCA [74]	×			×		870	4
CASA-MIA [75]	×	800 MeV				870	4
DICE [76]	×	800 MeV		×		860	1
EAS-Top [77]	×	1 GeV				820	−11
HEGRA [78]	×			×		790	−10
KASCADE (electrons/muons) [79]	×	230 MeV				1022	−7
KASCADE (hadrons/muons) [80]		230 MeV	50 GeV			1022	−1
KASCADE (neural network) [81]	×	230 MeV				1022	−8
MSU [82]	×					1020	−5
Mt. Norikura [83]	×					735	9
Tibet [84]	×					606	−10
Tunka-13 [85]				×		680	0
Yakutsk (low energy) [86]				×		1020	−3
AKENO (high energy) [87]	×					930	−16
Fly's Eye [88]					×	860	−3
Gauhati [89]	×					1025	−5
Haverah Park [90]	×					1018	−10
HiRes/MIA [91]		800 MeV			×	860	−5
Yakutsk (high energy) [92]	×	1 GeV		×		1020	−20

e: Electromagnetic, μ: muonic, h: hadronic, Č: Čerenkov, and F: fluorescence light. The particle thresholds are given for the muonic and hadronic components. In addition, the atmospheric overburden (g/cm^2) and the shift of the energy scale are listed.

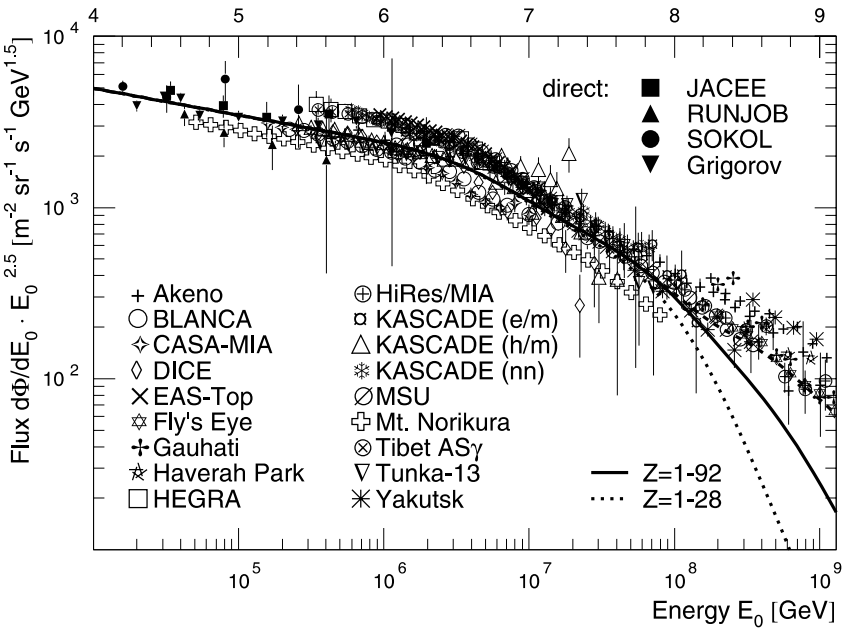

Fig. 8. All-particle energy spectra obtained from direct and indirect measurements, for references see Table 3 and text. The sum spectra for individual elements according to the poly-gonato model are represented by the dotted line for $1 \leqslant Z \leqslant 28$ and by the solid line for $1 \leqslant Z \leqslant 92$. Above 10^8 GeV the dashed line gives the normalized average spectrum.

Energy scales of individual experiments can be slightly shifted (within their systematic uncertainties). This yields a well defined all-particle energy spectrum.

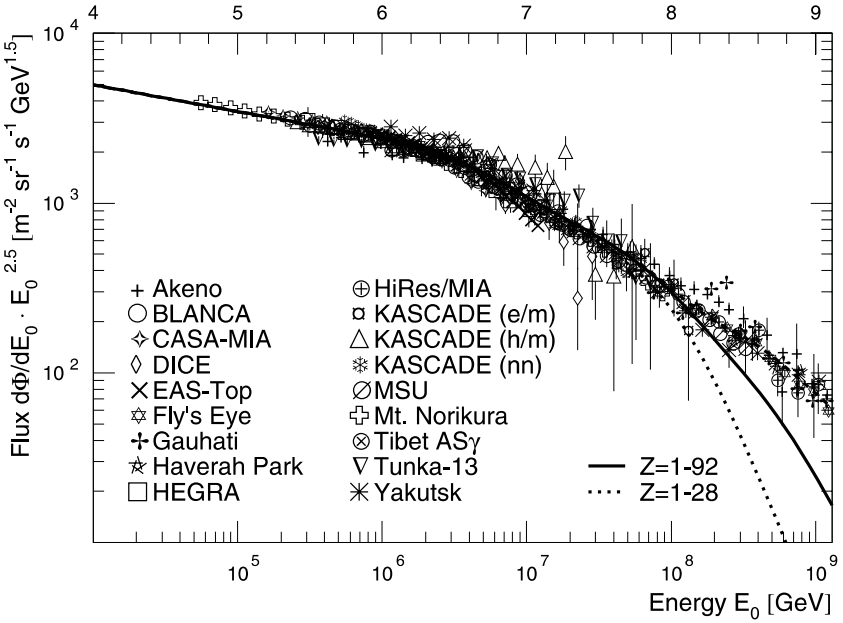

Fig. 10. Normalized all-particle energy spectra for individual experiments. The renormalization values for the energy scale and references are given in Table 3. The sum spectra for individual elements according to the poly-gonato model are represented by the dotted line for $1 \leqslant Z \leqslant 28$ and by the solid line for $1 \leqslant Z \leqslant 92$. Above 10^8 GeV the dashed line reflects the average spectrum.

all-particle energy spectrum is well defined

Possible reasons for the knee:

1) maximum energy attained during acceleration process in galactic sources

remember: $E_{max}^{SN} \sim Z \cdot R \cdot B \sim Z \cdot 10^{15}$ eV

expect:

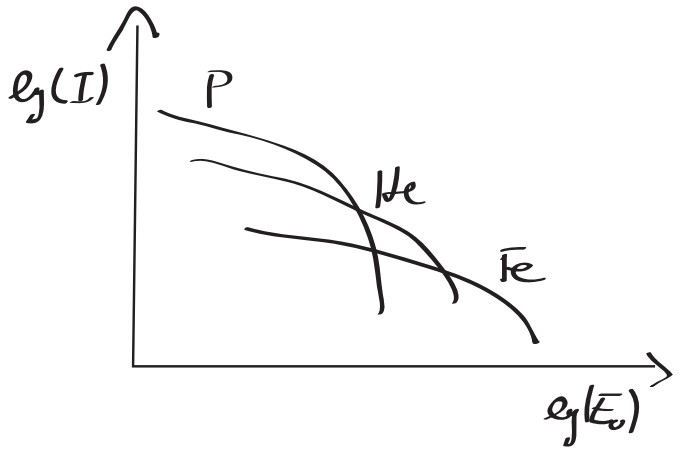

$E_c \propto Z$

2) Leakage from Galaxy – propagation effect

extrapolation of diffusion parameters to 10^{15} eV

$\tau_{esc}(E) \propto E^{\delta}$ $\quad \delta \simeq -0,6$

$\rightarrow c\,\tau_{esc}(10^{18}\,\text{eV}) \sim 300\,\text{pc}$ corresponds to thickness of galactic disc

$\rightarrow$ cosmic rays cannot be magnetically bound to Galaxy at high energies $E > E_k$

expect: same behavior of energy spectra as in 1) $E_k \propto Z$

& anisotropy of the arrival direction of cosmic rays more particles from the direction of the galactic plane

in addition to these astrophysical models also particle physic models are mentioned in the literature:

3) Interactions with background particles

e.g. interactions with heavy neutrinos from the diffuse neutrino background in the Galaxy

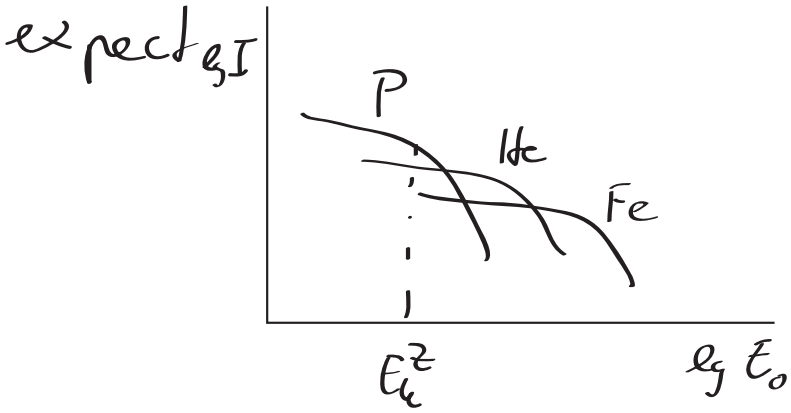

$E_c \propto A$

cross section for interaction depends on $\frac{E}{A}$ energy per nucleon → mass dependent cut-off

4/ New physics in the atmosphere

new interactions are postulated at high energies

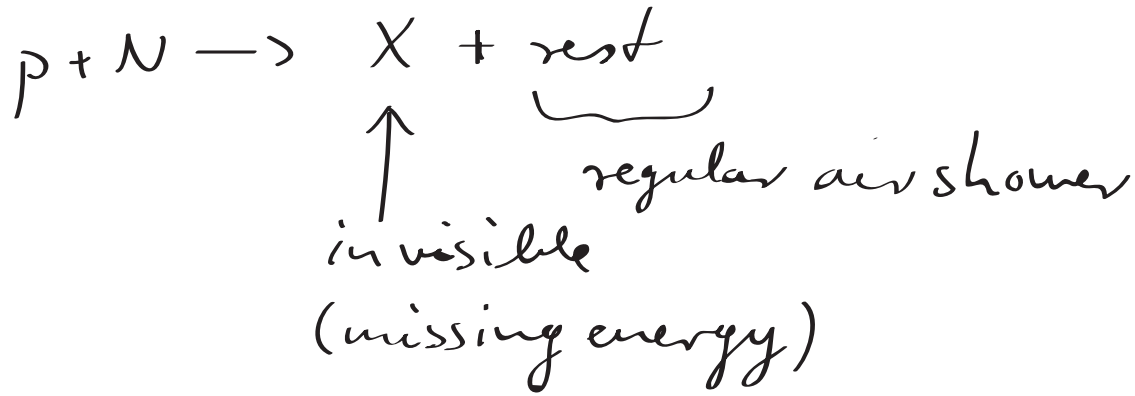

a fraction of the shower energy is transported into invisible channels

—> investigation of hadronic interaction models

Table 2
Synopsis of all models discussed

Model	Author(s)
Source/Acceleration	
Acceleration in SNR	Berezhko and Ksenofontov [18]
Acceleration in SNR + radio galaxies	Stanev et al. [19]
Acceleration by oblique shocks	Kobayakawa et al. [20]
Acceleration in variety of SNR	Sveshnikova [21]
Single source model	Erlykin and Wolfendale [22]
Reacceleration in the galactic wind	Völk and Zirakashvili [23]
Cannonball model	Plaga [24]
Propagation/Leakage from Galaxy:	
Minimum pathlength model	Swordy [25]
Anomalous diffusion model	Lagutin et al. [26]
Hall diffusion model	Ptuskin et al. [27], Kalmykov and Pavlov [42]
Diffusion in turbulent magnetic fields	Ogio and Kakimoto [28]
Diffusion and drift	Roulet et al [29]
Interactions with background particles	
Diffusion model + photo-disintegration	Tkaczyk [30]
Interaction with neutrinos in galactic halo	Dova et al. [31]
Photo-disintegration (optical and UV photons)	Candia et al. [32]
New interactions in the atmosphere	
Gravitons, SUSY, technicolor	Kazanas and Nicolaidis [33,34]

key observables in experiments are

- all-particle energy spectrum
- elemental composition
  - energy spectra for groups of elements
  - mean (logarithmic) mass
- anisotropy
- test of hadronic interactions

results of the KASCADE experiment:

use $N_e - N_\mu$ data to unfold energy spectra for groups of elements

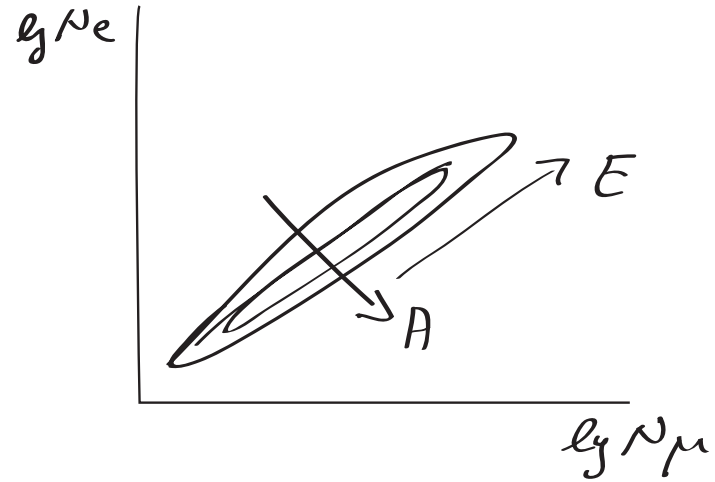

energy spectra for groups of elements

→ light elements show a depression of the flux at energies $E > E_k$

→ knee in the all-particle energy spectrum is caused by a cut-off of the light elements

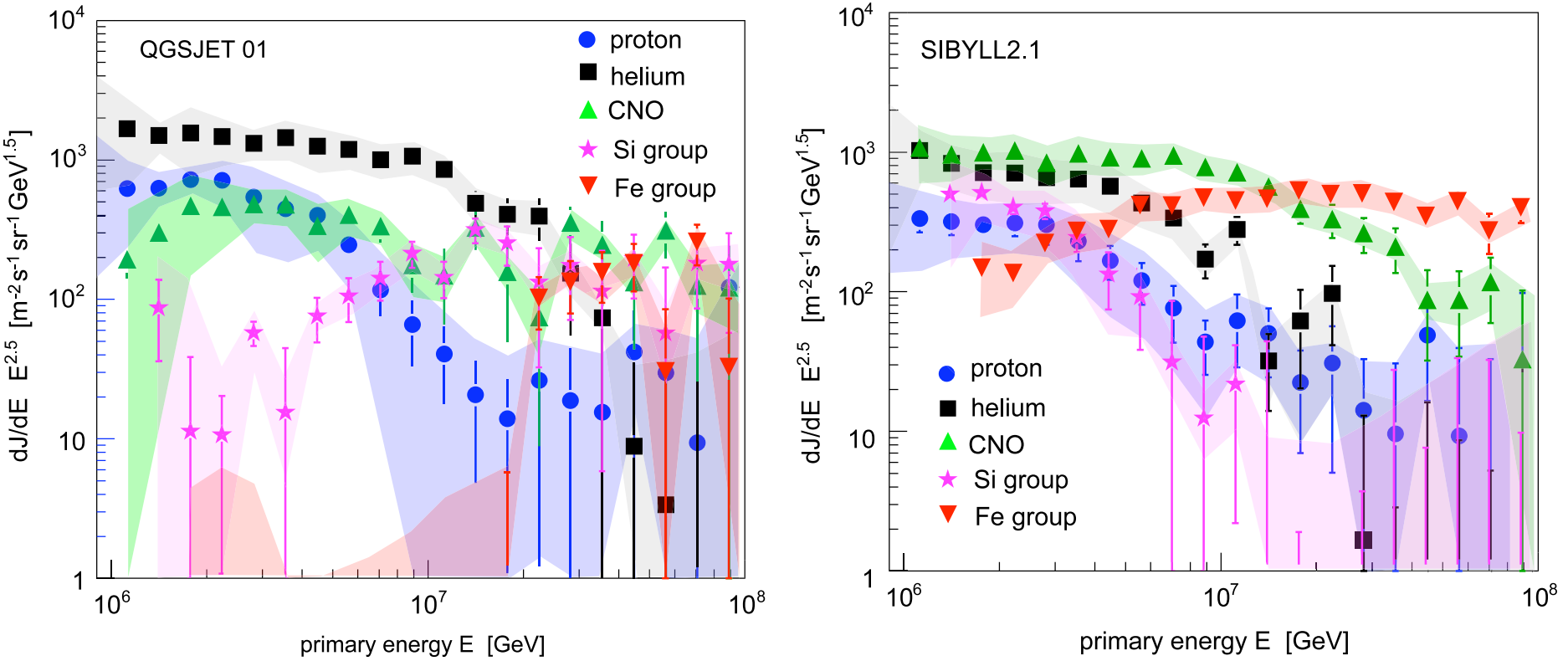

Fig. 15. Cosmic-ray energy spectrum for five groups of elements as reconstructed by the KASCADE experiment using the hadronic interaction models QGSJET 01 (*left*) and SIBYLL 2.1 (*right*) to interpret the measured data [224].

Energy spectra for groups of elements, according to KASCADE.

energy spectra for individual elements/ groups of elements

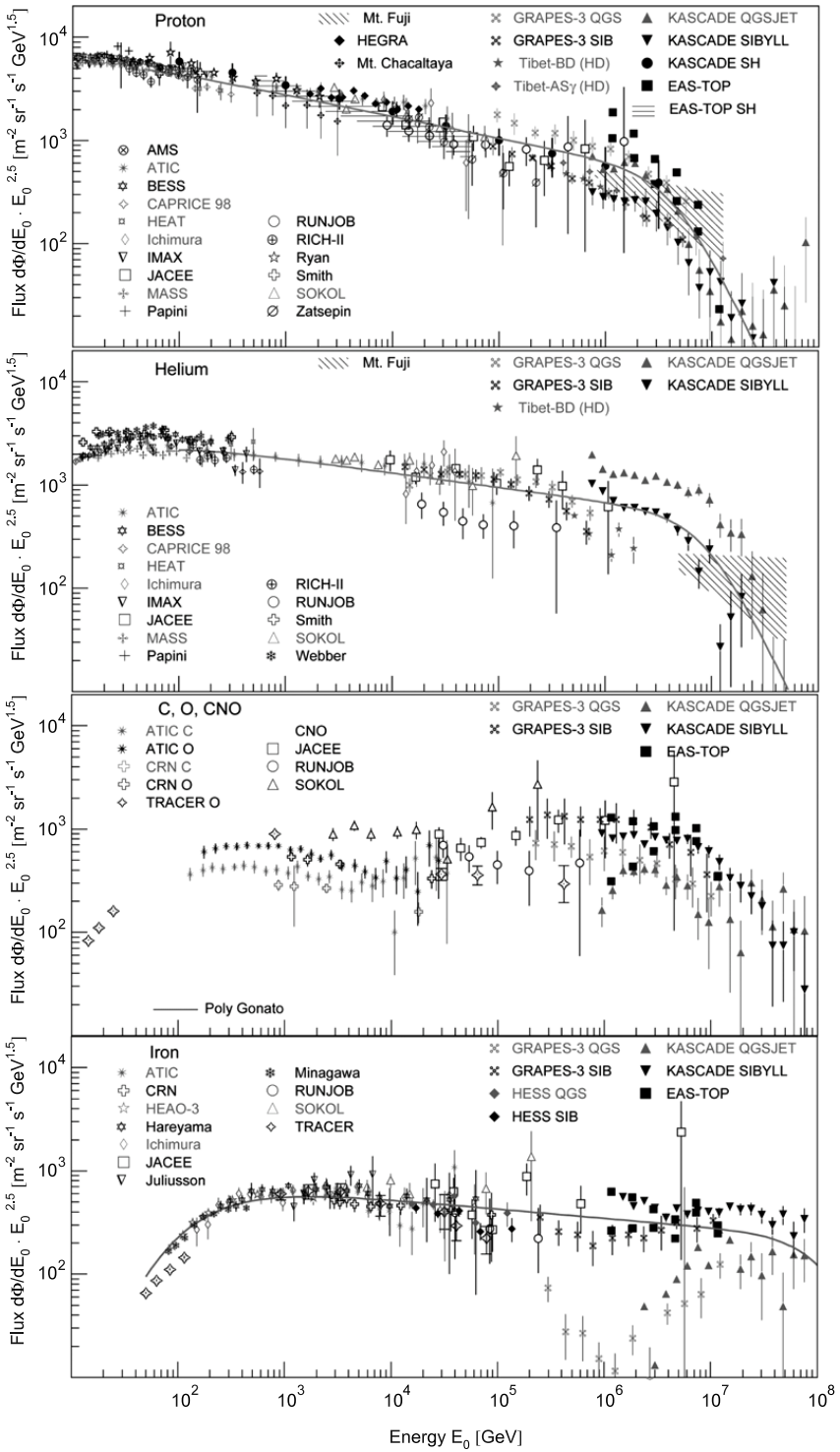

Fig. 9. Cosmic-ray energy spectra for four groups of elements, from top to bottom: protons, helium, CNO group, and iron group. **Protons:** Results from direct measurements above the atmosphere by AMS [242], ATIC [243], BESS [244], CAPRICE [245], HEAT [246,247], IMAX [248], JACEE [249], MASS [250,251], RUNJOB [222], RICH-II [252–254], SOKOL [231,255], and fluxes obtained from indirect measurements by KASCADE electrons and muons for two hadronic interaction models [224] and single hadrons [256], EAS-TOP (electrons and muons) [257] and single hadrons [258], GRAPES-3 interpreted with two hadronic interaction models [259], HEGRA [260], Mt. Chacaltaya [261], Mts. Fuji and Kanbala [262], Tibet burst detector (HD) [263] and ASγ (HD) [264]. **Helium:** Results from direct measurements above the atmosphere by ATIC [243], BESS [244], CAPRICE [245], HEAT [246,247], IMAX [248], JACEE [249], MASS [250,251], RICH-II [252], RUNJOB [222,254], SOKOL [231,265], and fluxes obtained from indirect measurements by KASCADE electrons and muons for two hadronic interaction models [224], GRAPES-3 interpreted with two hadronic interaction models [259], Mts. Fuji and Kanbala [262], and Tibet burst detector (HD) [263]. **CNO group:** Results from direct measurements above the atmosphere by ATIC (C + O) [266], CRN (C+O) [267], TRACER (O) [268], JACEE (CNO) [269], RUNJOB (CNO) [222], SOKOL (CNO) [231], and fluxes obtained from indirect measurements by KASCADE electrons and muons [224], GRAPES-3 [259], the latter two give results for two hadronic interaction models, and EAS-TOP [257]. **Iron:** Results from direct measurements above the atmosphere by ATIC [266], CRN [267], HEAO-3 [270–272], TRACER [268] (single element resolution) and [273,247], JACEE [230], RUNJOB [222], SOKOL [231] (iron group), as well as fluxes from indirect measurements (iron group) by EAS-TOP [257], KASCADE electrons and muons [224], GRAPES-3 [259], and H.E.S.S. direct Cherenkov light [274]. The latter three experiments give results according to interpretations of the measured air-shower data with two hadronic interaction models, namely QGSJET and SIBYLL. The gray solid lines indicate spectra according to the poly-gonato model [2].

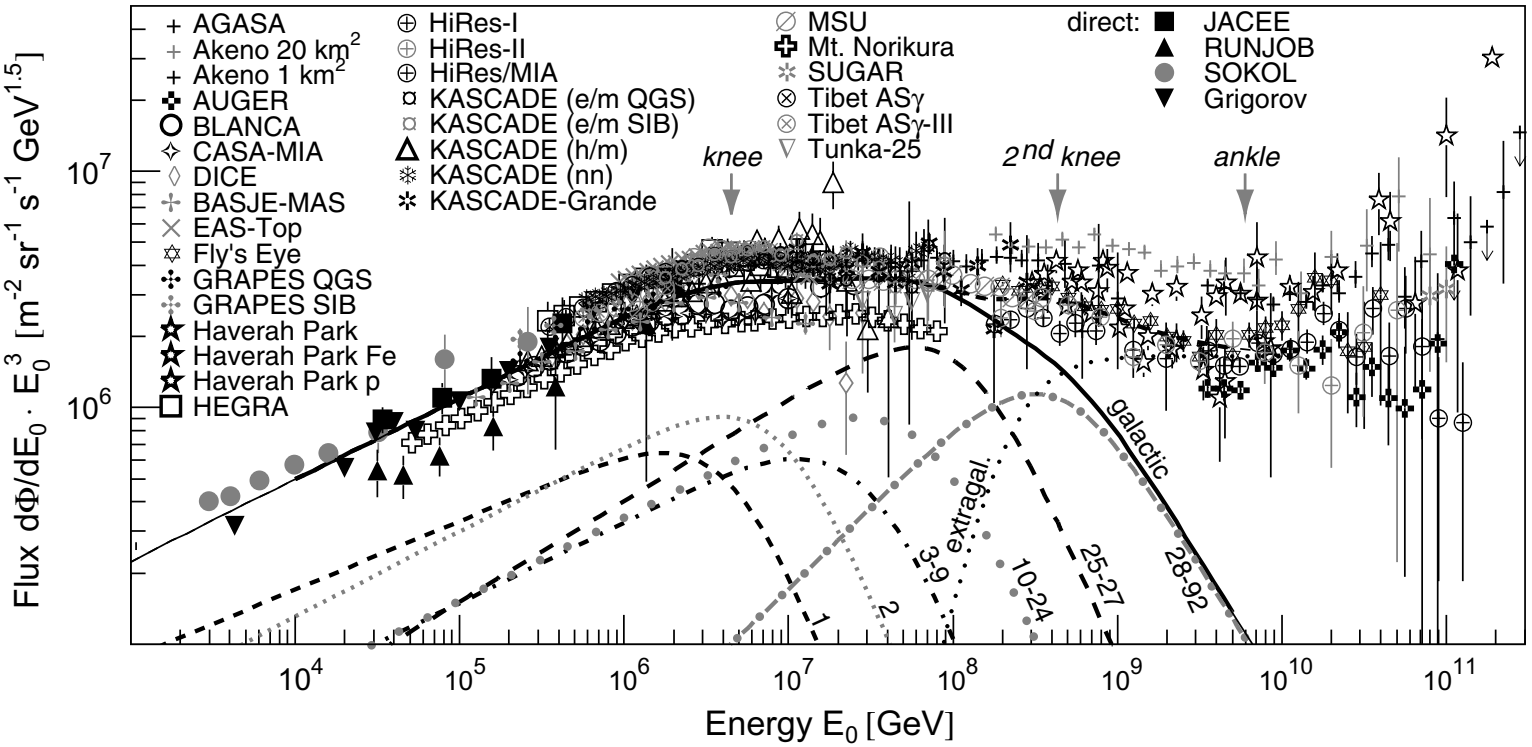

Fig. 8. All-particle energy spectrum of cosmic rays, the flux is multiplied by E^3. Results from direct measurements by Grigorov et al. (1999), JACEE (Asakimori et al., 1995), RUNJOB (Derbina et al., 2005), and SOKOL (Ivanenko et al., 1993) as well as from the air shower experiments AGASA (Takeda et al., 2003), Akeno 1 km^2 (Nagano et al., 1984a), and 20 km^2 (Nagano et al., 1984b), AUGER (Sommers et al., 2005), BASJE-MAS (Ogio et al., 2004), BLANCA (Fowler et al., 2001), CASA-MIA (Glasmacher et al., 1999b), DICE (Swordy and Kieda, 2000), EAS-TOP (Aglietta et al., 1999), Fly's Eye (Corbato et al., 1994), GRAPES-3 interpreted with two hadronic interaction models (Hayashi et al., 2005), Haverah Park (Lawrence et al., 1991) and (Ave et al., 2003), HEGRA (Arqueros et al., 2000), HiRes–MIA (Abu-Zayyad et al., 2001a), HiRes-I (Abbasi et al., 2004), HiRes-II (Abbasi et al., 2005), KASCADE electrons and muons interpreted with two hadronic interaction models (Antoni et al., 2005), hadrons (Hörandel et al., 1999), and a neural network analysis combining different shower components (Antoni et al., 2002), KASCADE-Grande (preliminary) (Haungs et al., in press), MSU (Fomin et al., 1991), Mt. Norikura (Ito et al., 1997), SUGAR (Anchordoqui and Goldberg, 2004), Tibet ASγ (Amenomori et al., 2000a) and ASγ-III (Amenomori et al., 2003), Tunka-25 (Chernov et al., 2006), and Yakutsk (Glushkov et al., 2003). The lines represent spectra for elemental groups (with nuclear charge numbers Z as indicated) according to the poly-gonato model (Hörandel, 2003a). The sum of all elements (galactic) and a presumably extragalactic component are shown as well. The dashed line indicates the average all-particle flux at high energies.

The all-particle flux can be described as the sum of the spectra of individual elements.

compilation of the world data set for the energy spectra of individual elements / groups of elements cut-off compatible with $E_k \propto Z$

all-particle energy spectrum can be described as sum of the spectra for individual elements with $E_k \propto Z$

a detailed comparison to the predictions of models to explain the knee with experimental data indicates:

data are compatible with scenarios 1) and 2) above, i.e. maximum energy and leakage from Galaxy

models to explain the knee in the energy spectrum due to maximum energy achieved in accelerators

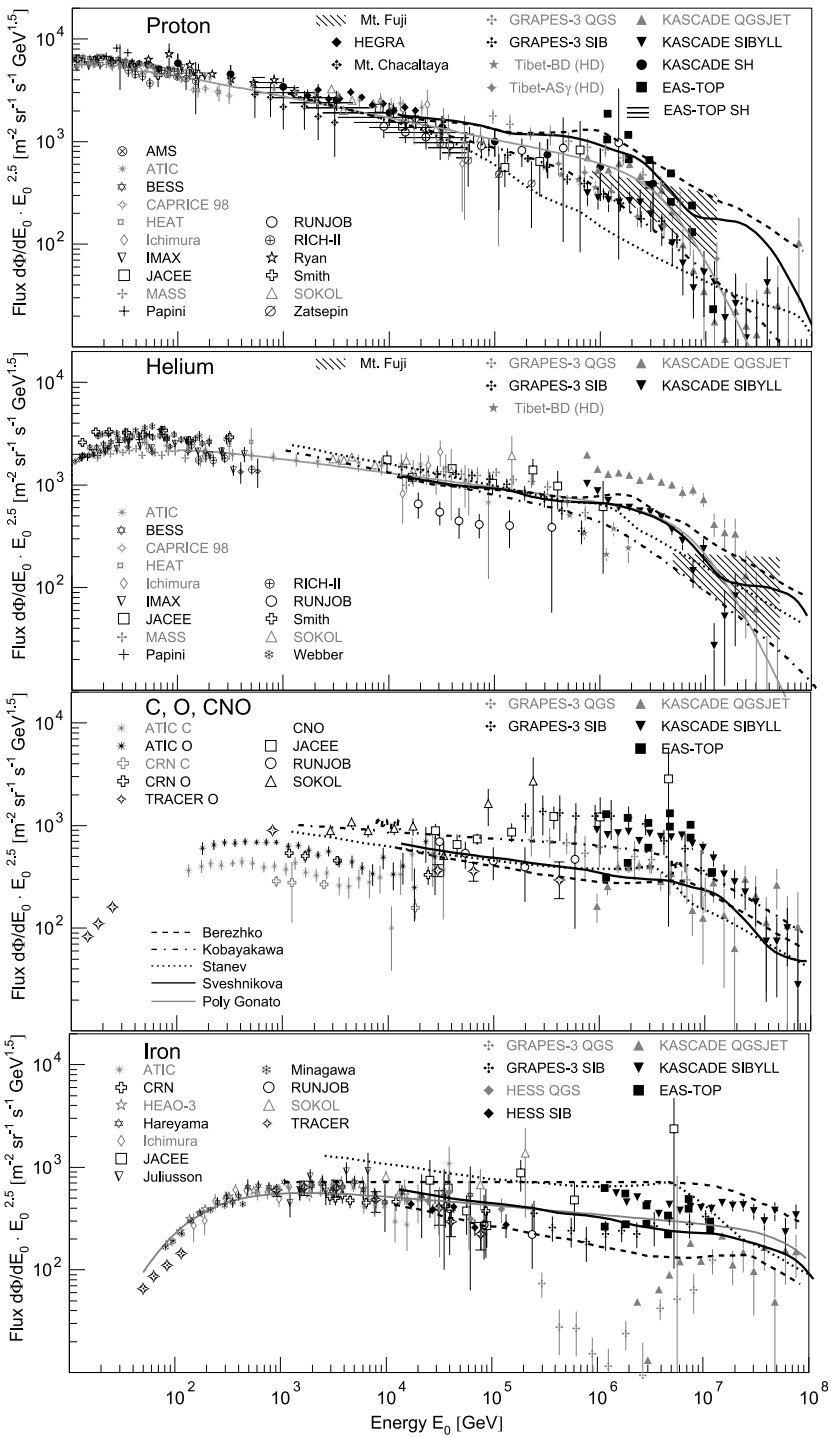

Fig. 13. Cosmic-ray energy spectra for four groups of elements, from top to bottom: protons, helium, CNO group, and iron group.

Protons: Results from direct measurements above the atmosphere by AMS (Alcaraz et al., 2000), ATIC (Wefel et al., 2005), BESS (Sanuki et al., 2000), CAPRICE (Boezio et al., 2003), HEAT (Vernois et al., 2001), Ichimura et al., 1993, IMAX (Menn et al., 2000), JACEE (Asakimori et al., 1998), MASS (Bellotti et al., 1999), Papini et al., 1993, RUNJOB (Derbina et al., 2005), RICH-II (Diehl et al., 2003), Ryan et al., 1972, Smith et al., 1973, SOKOL (Ivanenko et al., 1993), Zatsepin et al., 1993, and fluxes obtained from indirect measurements by KASCADE electrons and muons for two hadronic interaction models (Antoni et al., 2005) and single hadrons (Antoni et al., 2004b), EAS-TOP (electrons and muons) (Navarra et al., 2003) and single hadrons (Aglietta et al., 2003), GRAPES-3 interpreted with two hadronic interaction models (Hayashi et al., 2005), HEGRA (Aharonian et al., 1999), Mt. Chacaltaya (Inoue et al., 1997), Mts. Fuji and Kanbala (Huang et al., 2003), Tibet burst detector (HD) (Amenomori et al., 2000b) and ASγ (HD) (Amenomori et al., 2004).

Helium: Results from direct measurements above the atmosphere by ATIC (Wefel et al., 2005), BESS (Sanuki et al., 2000), CAPRICE (Boezio et al., 2003), HEAT (Vernois et al., 2001), Ichimura et al. (1993), IMAX (Menn et al., 2000), JACEE (Asakimori et al., 1998), MASS (Bellotti et al., 1999), Papini et al. (1993), RICH-II (Diehl et al., 2003), RUNJOB (Derbina et al., 2005), Smith et al. (1973), SOKOL (Ivanenko et al., 1993), Webber et al. (1987), and fluxes obtained from indirect measurements by KASCADE electrons and muons for two hadronic interaction models (Antoni et al., 2005), GRAPES-3 interpreted with two hadronic interaction models (Hayashi et al., 2005), Mts. Fuji and Kanbala (Huang et al., 2003), and Tibet burst detector (HD) (Amenomori et al., 2000b).

CNO group: Results from direct measurements above the atmosphere by ATIC (C + O) (Cherry, 2006), CRN (C + O) (Müller et al., 1991), TRACER (O) (Müller et al., 2005), JACEE (CNO) (JACEE collaboration, 1999), RUNJOB (CNO) (Derbina et al., 2005), SOKOL (CNO) (Ivanenko et al., 1993), and fluxes obtained from indirect measurements by KASCADE electrons and muons (Antoni et al., 2005), GRAPES-3 (Hayashi et al., 2005), the latter two give results for two hadronic interaction models, and EAS-TOP (Navarra et al., 2003).

Iron: Results from direct measurements above the atmosphere by ATIC (Cherry, 2006), CRN (Müller et al., 1991), HEAO-3 (Engelmann et al., 1985), Juliusson (1974), Minagawa (1981), TRACER (Müller et al., 2005) (single-element resolution) and Hareyama et al. (1999), Ichimura et al. (1993), JACEE (Asakimori et al., 1995), RUNJOB (Derbina et al., 2005), SOKOL (Ivanenko et al., 1993) (iron group), as well as fluxes from indirect measurements (iron group) by EAS-TOP (Navarra et al., 2003), KASCADE electrons and muons (Antoni et al., 2005), GRAPES-3 (Hayashi et al., 2005), and HESS direct Čerenkov light (Aharonian et al., 2007). The latter three experiments give results according to interpretations with two hadronic interaction models.

Models: The the grey solid lines indicate spectra according to the poly-gonato model (Hörandel, 2003a).The black lines indicate spectra for models explaining the knee due to the maximum energy attained during the acceleration process according to Sveshnikova (2003) (—), Berezhko and Ksenofontov (1999) (- - -), Stanev et al. (1993) (···), and Kobayakawa et al. (2002) (-·-·-).

models to explain the knee in the energy spectrum due to leakage from Galaxy

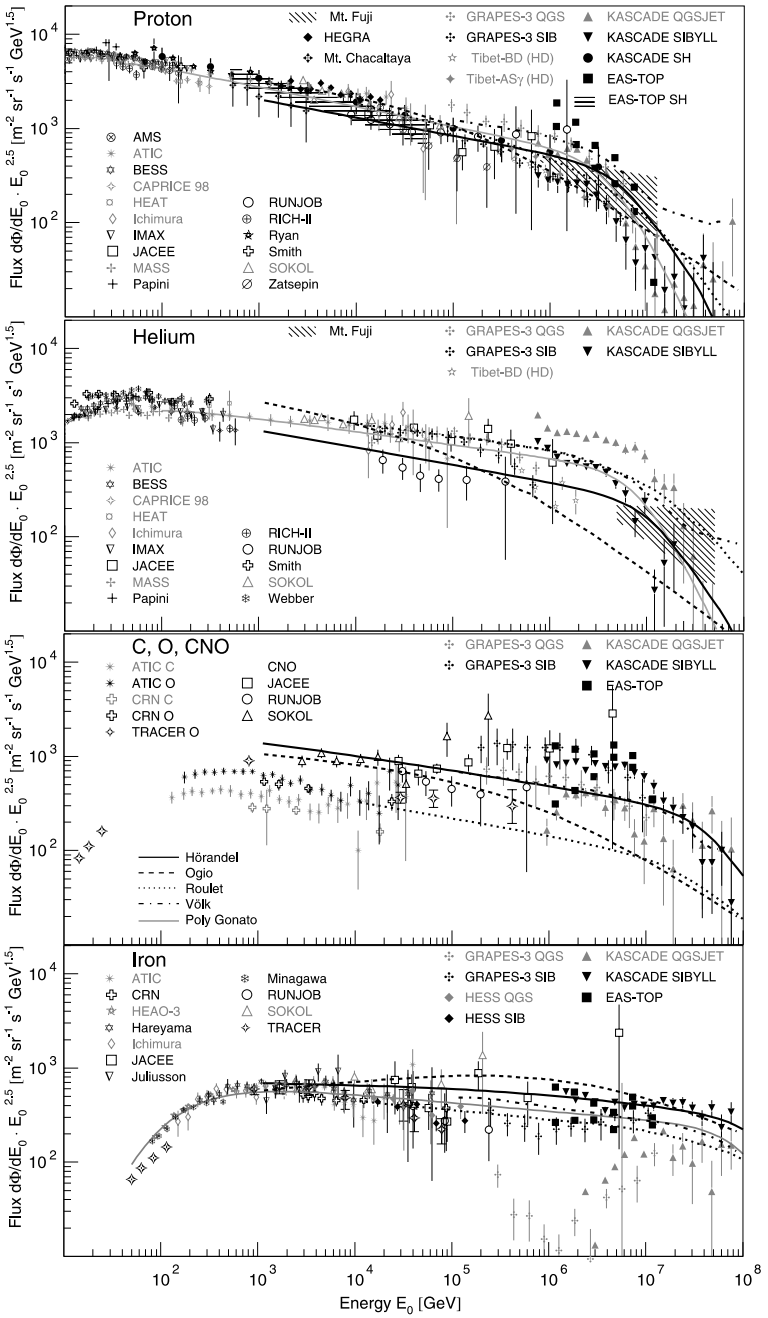

Fig. 14. Cosmic-ray energy spectra for four groups of elements, from top to bottom: protons, helium, CNO group, and iron group. (Refer to note in Fig. 13.) The grey solid lines indicate spectra according to the poly-gonato model (Hörandel, 2003a). The black lines indicate spectra for models explaining the knee as effect of leakage from the Galaxy during the propagation process according to Hörandel et al. (2007) (—), Ogio and Kakimoto (2003) (- - -), Roulet (2004) (···), as well as Völk and Zirakashvili (2003) (-·-·-).

mass composition

average depth of the shower maximum

mean logarithmic mass

$$\langle \ln A \rangle = \sum_i r_i \ln A_i \qquad r_i \text{ relative fraction of element } i$$

$$\langle \ln A \rangle = \frac{X_{max}^{meas} - X_{max}^{p}}{X_{max}^{Fe} - X_{max}^{p}} \ln A_{Fe}$$

Both, $\langle \ln A \rangle$ values derived from X_{max} as well as from N_e/N_μ ratio exhibit an increase of $\langle \ln A \rangle$ as function of energy in the energy range 1 PeV - 100 PeV

→ indication for the cut-off of light elements at the knee

average depth of the shower maximum X_{max}

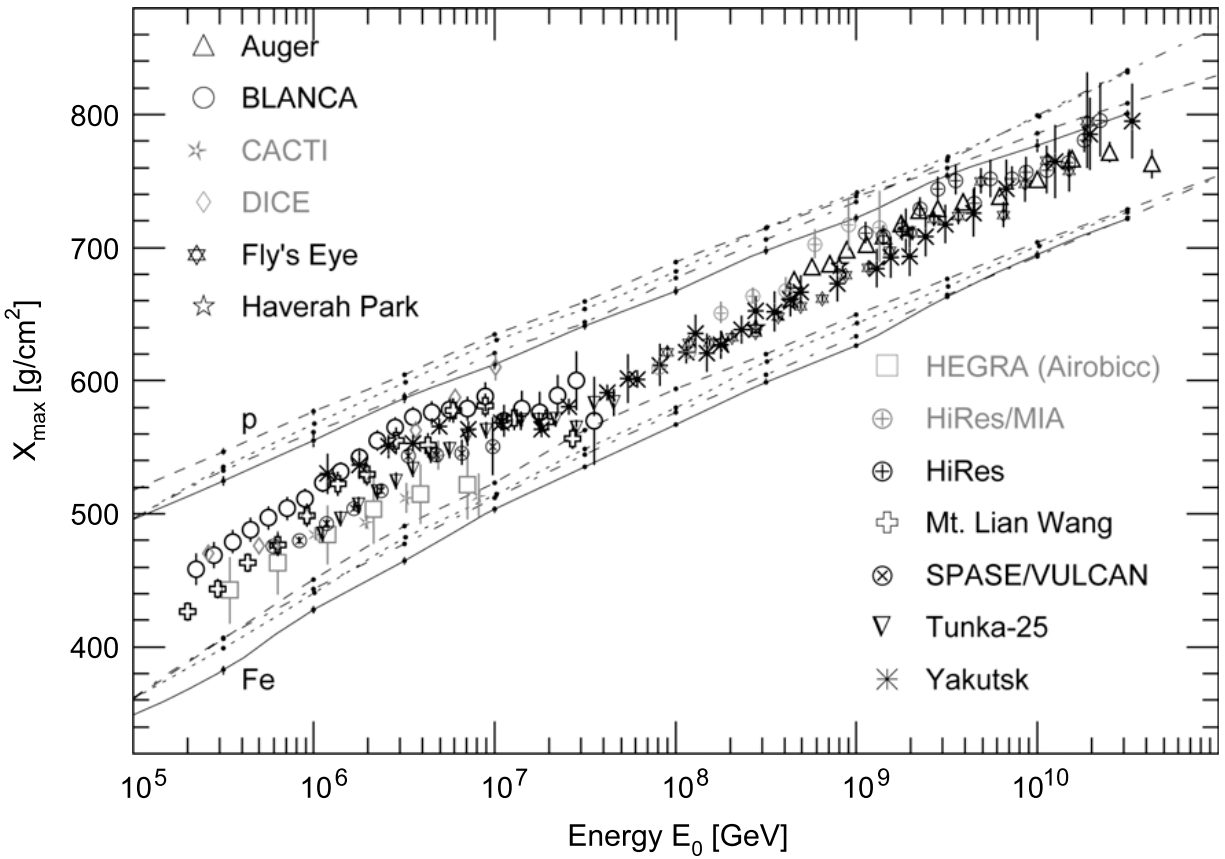

Fig. 13. Average depth of the shower maximum X_{max} as function of primary energy as obtained by Auger [305], BLANCA [173], CACTI [306], DICE [182], Fly's Eye [307], Haverah Park [308], HEGRA [174], HiRes/MIA [228], HiRes [309], Mt. Lian Wang [310], SPASE/VULCAN [311], Tunka-25 [176], Yakutsk [312]. The lines indicate simulations for proton and iron induced showers using the CORSIKA code with the hadronic interaction model QGSJET 01 (—), QGSJET II-3 (- - -), SIBYLL 2.1 (. . .), and EPOS 1.6 (-·-·).

mean logarithmic mass derived from X_{max} measurements

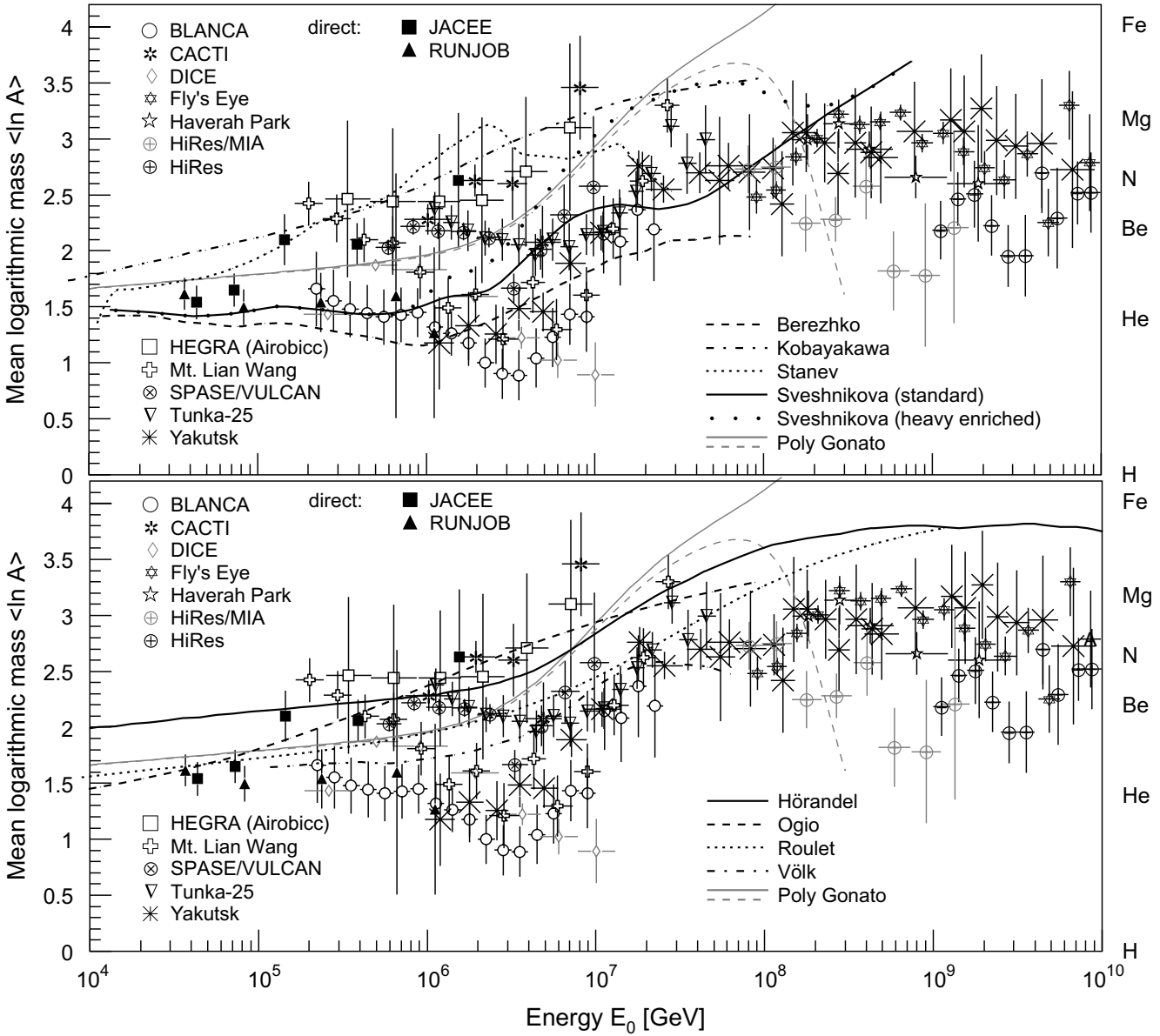

Fig. 12. Mean logarithmic mass of cosmic-rays derived from the average depth of the shower maximum, see Fig. 10. As hadronic interaction model used to interpret the measurements serves a modified version of QGSJET 01 with lower cross sections and a slightly increased elasticity (model 3a Hörandel, 2003b). For experimental references, see caption in Fig. 10. For comparison, results from direct measurements are shown as well from the JACEE (JACEE collaboration, 1999) and RUNJOB (Derbina et al., 2005) experiments. *Models:* The grey solid and dashed lines indicate spectra according to the poly-gonato model (Hörandel, 2003a). Top: The lines indicate spectra for models explaining the knee due to the maximum energy attained during the acceleration process according to Sveshnikova (2003) (—, · · ·), Berezhko and Ksenofontov (1999) (- - -), Stanev et al. (1993) (· · ·), Kobayakawa et al. (2002) (-·-·-). Bottom: The lines indicate spectra for models explaining the knee as effect of leakage from the Galaxy during the propagation process according to Hörandel et al. (2007) (—), Ogio and Kakimoto (2003) (- - -), Roulet (2004) (· · ·), as well as Völk and Zirakashvili (2003) (-·-·-).

mean logarithmic mass derived from the measurement of electrons, muons, and hadrons at ground level

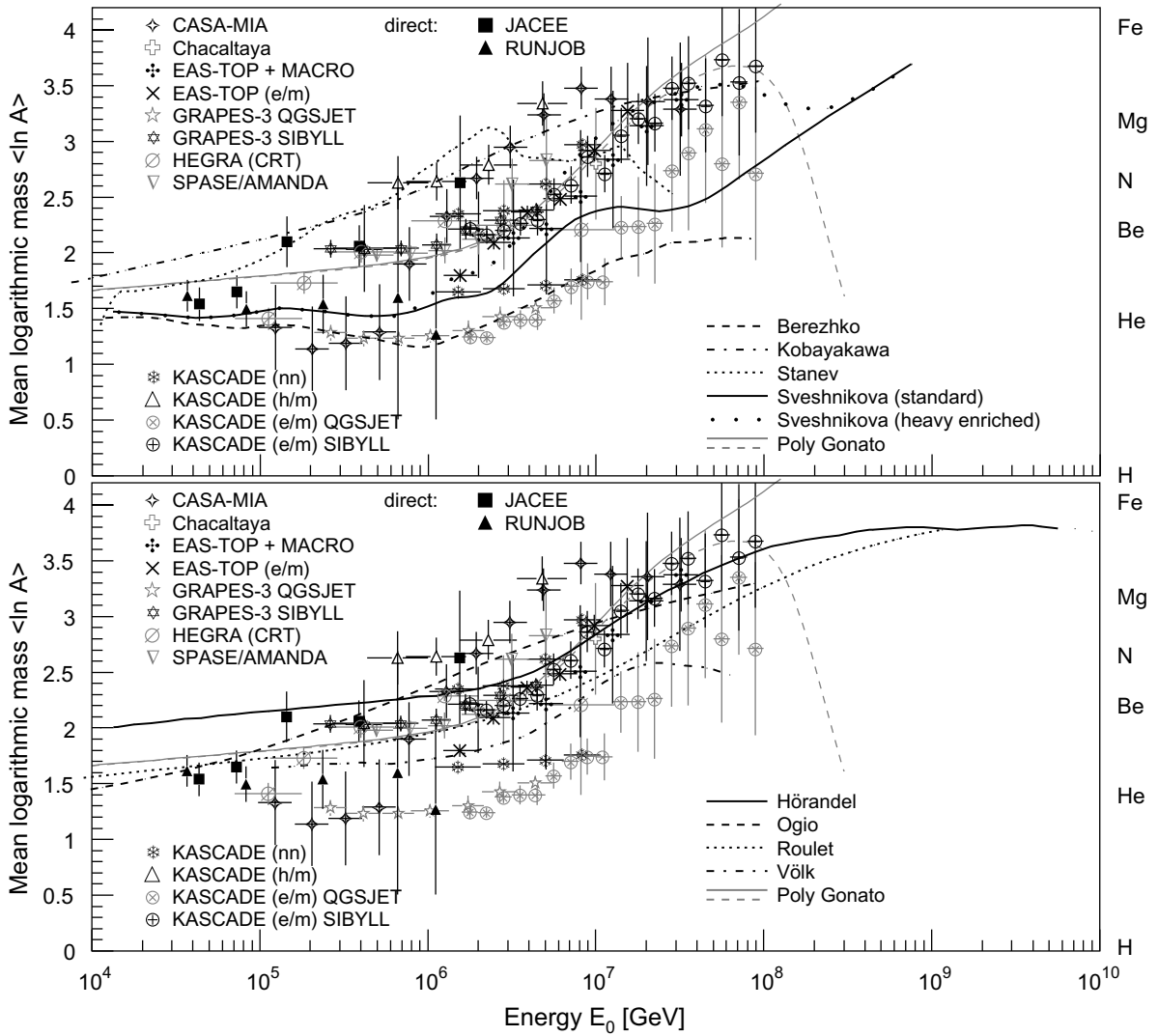

Fig. 9. Mean logarithmic mass of cosmic-rays derived from the measurements of electrons, muons, and hadrons at ground level. Results are shown from CASA-MIA (Glasmacher et al., 1999a), Chacaltaya (Aguirre et al., 2000), EAS-TOP electrons and GeV muons (Aglietta et al., 2004a), EAS-TOP/MACRO (TeV muons) (Aglietta et al., 2004b), GRAPES-3 data interpreted with two hadronic interaction models (Hayashi et al., 2005), HEGRA CRT (Bernlöhr et al., 1998), KASCADE electrons and muons interpreted with two hadronic interaction models (Antoni et al., 2005), hadrons and muons (Hörandel, 1998), as well as an analysis combining different observables with a neural network (Antoni et al., 2002), and SPASE/AMANDA (Rawlins et al., 2003). For comparison, results from direct measurements are shown as well from the JACEE (JACEE collaboration, 1999) and RUNJOB (Derbina et al., 2005) experiments. For orientation, ln A for selected elements is indicated on the right-hand side. *Models:* The grey solid and dashed lines indicate spectra according to the poly-gonato model (Hörandel, 2003a). Top: The lines indicate spectra for models explaining the knee due to the maximum energy attained during the acceleration process according to Sveshnikova (2003) (—, ···), Berezhko and Ksenofontov (1999) (---), Stanev et al. (1993) (···), Kobayakawa et al. (2002) (-·-·-). Bottom: The lines indicate spectra for models explaining the knee as effect of leakage from the Galaxy during the propagation process according to Hörandel et al. (2007) (—), Ogio and Kakimoto (2003) (---), Roulet (2004) (···), as well as Völk and Zirakashvili (2003) (-·-·-).

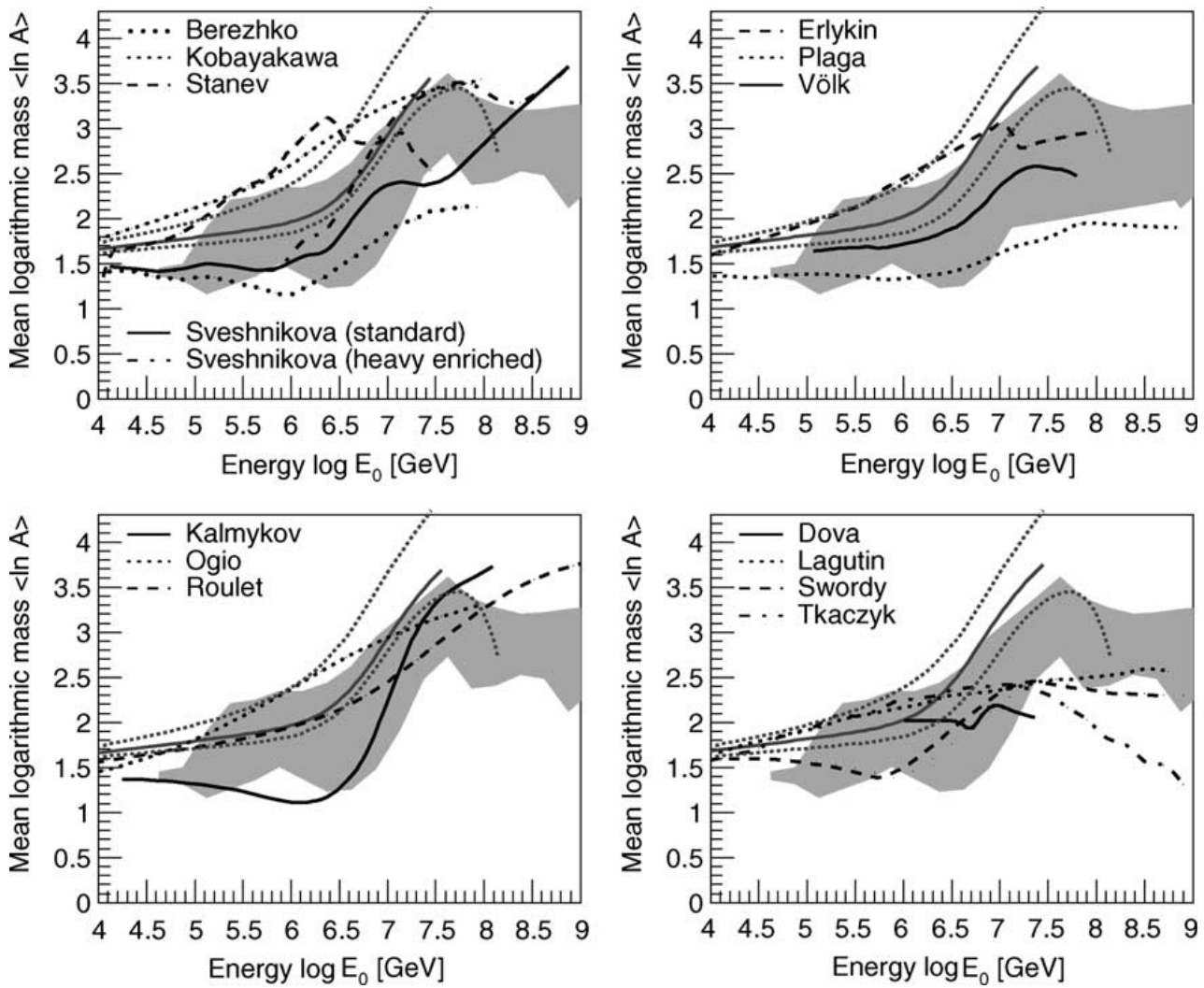

Fig. 4. Mean logarithmic mass derived from many experiments (shaded area) compared to $\langle \ln A \rangle$ as obtained with different models. (Upper left panel) Acceleration in supernova remnants as described by Berezhko and Ksenofontov [18], Kobayakawa et al. [20], Stanev et al. [19], and Sveshnikova [21]; (upper right panel) source and acceleration related models by Erlykin and Wolfendale [22], Plaga [24], as well as Völk and Zirakashvili [23]; (lower left panel) diffusion models by Kalmykov et al. [42], Ogio and Kakimoto [28], as well as Roulet et al. [29] and (lower right panel) propagation models by Dova et al. [31], Lagutin et al. [26], Swordy [25], and Tkaczyk [30]. In addition, the range of $\langle \ln A \rangle$ for the extrapolation of direct measurements according to the *poly-gonato* model is indicated as dotted grey lines, see text.

- models according to scenarios 1) & 2) are compatible with the measurements
- scenario 3) yields a light composition at energies 10 PeV – 100 PeV which is not observed
- tests of hadronic interaction models with air shower data yield no evidence for scenario 4)

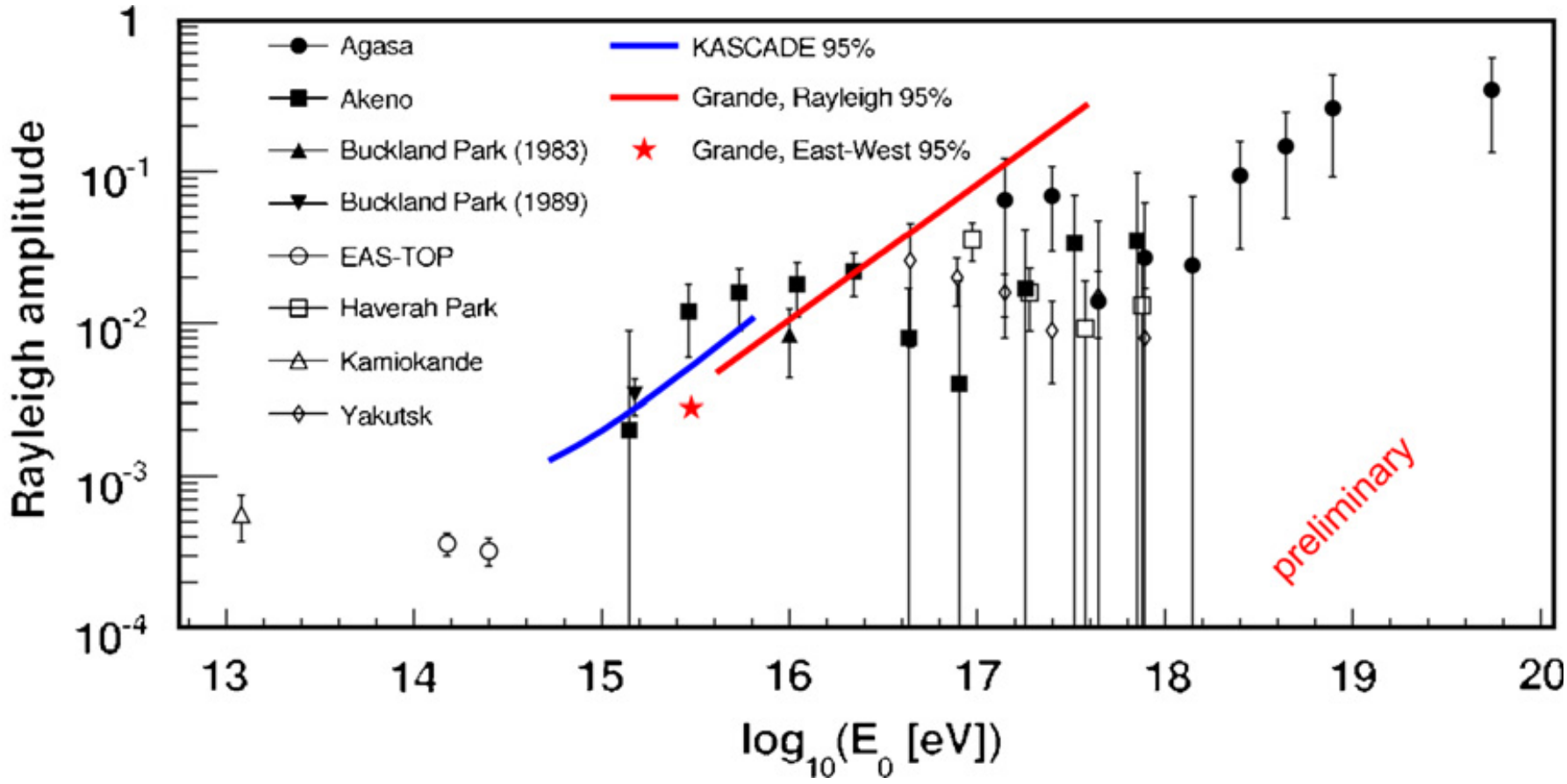

Fig. 6. Rayleigh amplitudes as function of energy as observed by different experiments [39].

(an)isotropy of the arrival direction of cosmic rays

anisotropy of the arrival directions

the observed anisotropy is compatible with scenarios 2) (leakage from Galaxy)

Summary

- no (big) inconsistencies in the description of hadronic interactions -> hence is astrophysical effect (no particle physics in atmosphere)

- increase of the mean (logarithmic) mass as function of energy

- strong indications for a rigidity ($\propto Z$) dependent cut-off of the spectra for groups of elements

$E_A \propto Z$

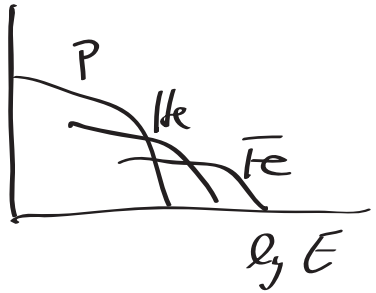

$\Rightarrow$ most likely the knee is caused by a combination of two (astrophysical) effects:

- maximum energy of the accelerators (supernovae)
- leakage from Galaxy

Transition from galactic to extragalactic cosmic rays

at energies between 10^{17} and 10^{18} eV all elements of the galactic cosmic-ray component should reach their cut-off energies

→ observed all-particle flux is mostly composed of particles from other galaxies (extragalactic cosmic rays)

Different scenarios are discussed in the literature, most expect a transition from galactic to extragalactic origin of the cosmic-ray particles at energies between 10^{17} and 10^{18} eV.

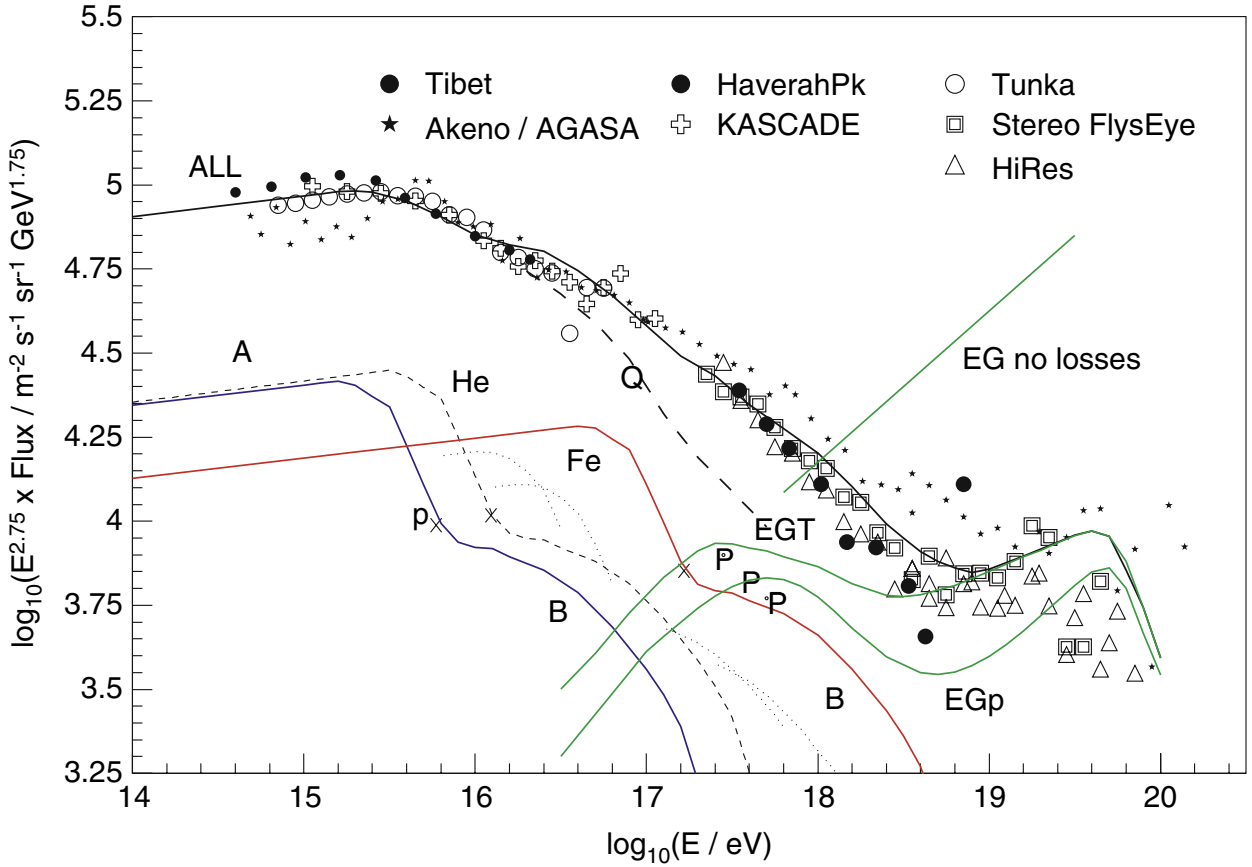

Fig. 25. The breakdown of the cosmic-ray spectrum according to a model of Hillas [449] as the sum of galactic H, He, CNO, Ne–S, and Fe components with the same rigidity dependence, and extragalactic H + He having a spectrum $\propto E^{-2.3}$ before suffering losses by cosmic microwave background and starlight interactions. The galactic components were given a turn-down shape based on a KASCADE knee shape as far as the point marked x. The dashed line Q is the total galactic SNR flux if the extended tail (component B) of the galactic flux is omitted [449].

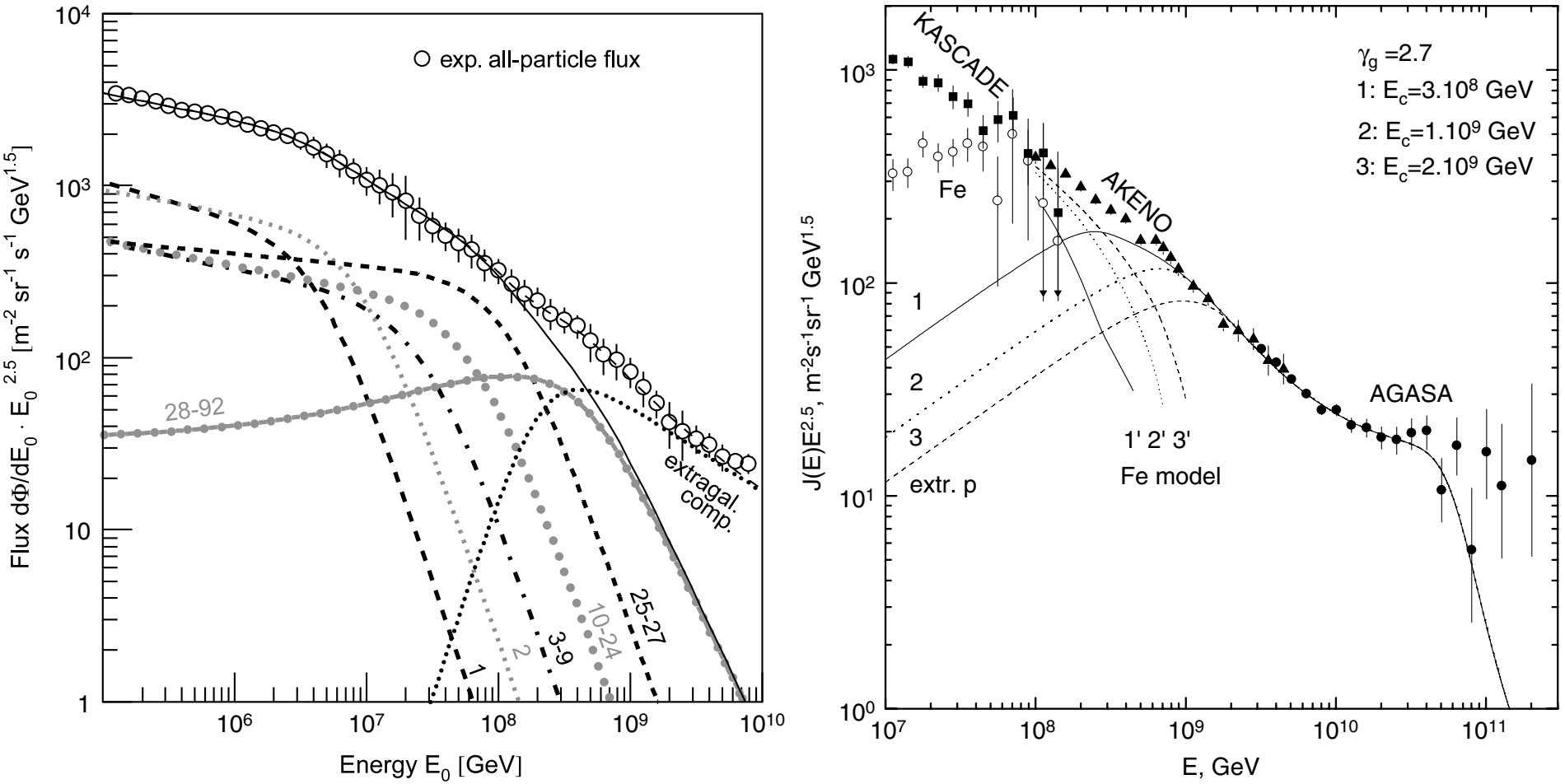

Fig. 26. *Left panel*: Cosmic-ray energy spectra according to the poly-gonato model [2]. The spectra for groups of elements are labeled by their respective nuclear charge numbers. The sum of all elements yields the galactic all-particle spectrum (—) which is compared to the average measured flux. In addition, a hypothetical extragalactic component is shown to account for the observed all-particle flux (- - -). *Right panel*: Transition from galactic to extragalactic cosmic rays according to Berezinsky et al. [451]. Calculated spectra of extragalactic protons (curves 1, 2, 3) and of galactic iron nuclei (curves 1′, 2′, 3′) are compared with the all-particle spectrum from the Akeno and AGASA experiments. KASCADE data are shown as filled squares for the all-particle flux and as open circles for the flux of iron nuclei.

The highest energy particles in the Universe

1962: first observation of a cosmic ray with $E > 10^{20}$ eV

10^{20} eV is a macroscopic energy: 50 J

Can such particles originate from our Galaxy?

Simple argument:

radius of trajectory of particles in B field

$$r = \frac{p}{ZeB} \qquad r(\mathrm{pc}) = 1{,}08 \; \frac{E(\mathrm{PeV})}{B(\mu\mathrm{G})}$$

→ particles above 10^{18} eV cannot be magnetically bound to galaxy

→ extragalactic origin

Vulcano Ranch, New Mexico, John Linsley

first EAS with 10^{20} eV measured 1962

Radius of particle in magnetic field

$$r = \frac{p}{ZeB} \qquad r[pc] = 1.08 * \frac{E\ [PeV]}{B\ [\mu G]}$$

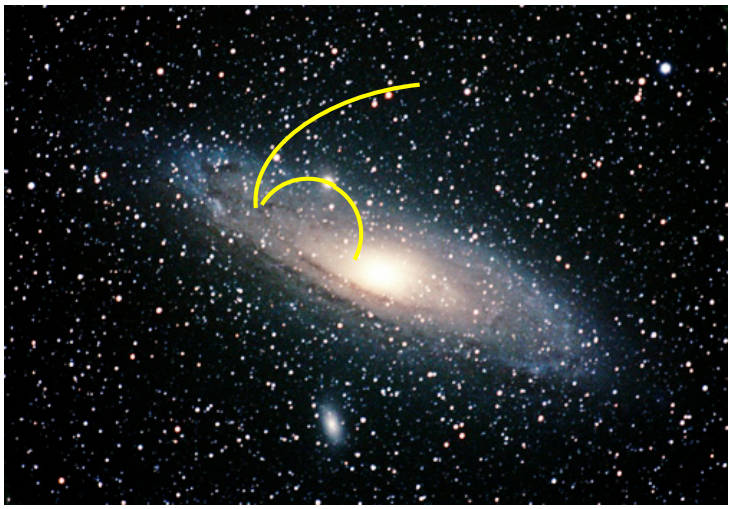

extragalactic cosmic rays

r= 0.04 pc 3.6 pc 360 pc 36 kpc